Human stem cell delivery for treatment of large segmental bone defects

Kenneth M. Dupont[a,b], Kapil Sharma[c], Hazel Y. Stevens[a,b], Joel D. Boerckel[a,b], Andrés J. García[a,b], and Robert E. Guldberg[a,b,1]

[a]George W. Woodruff School of Mechanical Engineering, Georgia Institute of Technology, Atlanta, GA 30332-0405; [b]Parker H. Petit Institute for Bioengineering and Biosciences, Georgia Institute of Technology, Atlanta, GA 30332-0363; and [c]College of Medicine, National University of Ireland, Galway, Ireland

Edited by Stephen F. Badylak, University of Pittsburgh Medical Center, Pittsburgh, PA, and accepted by the Editorial Board December 17, 2009 (received for review May 15, 2009)

Local or systemic stem cell delivery has the potential to promote repair of a variety of damaged or degenerated tissues. Although various stem cell sources have been investigated for bone repair, few comparative reports exist, and cellular distribution and viability postimplantation remain key issues. In this study, we quantified the ability of tissue-engineered constructs containing either human fetal or adult stem cells to enhance functional repair of nude rat critically sized femoral defects. After 12 weeks, defects treated with cell-seeded polymer scaffolds had significantly higher bone ingrowth and torsional strength compared to those receiving acellular scaffolds, although there were no significant differences between the cell sources. Next, stem cells were labeled with fluorescent quantum dots (QDs) in an attempt to noninvasively track their distribution after delivery on scaffolds. Clear fluorescence was observed at implantation sites throughout the study; however, beginning 7–10 days after surgery, signals were also observed at contralateral sites treated with acellular QD-free scaffolds. Although immunostaining for human nuclei revealed retention of some cells at the implantation site, no human cells were detected in the control limb defects. Additional histological analysis of implantation and control defect tissues revealed macrophages containing endocytosed QDs. Furthermore, QD-labeling appeared to diminish transplanted cell function resulting in reduced healing responses. In summary, augmentation of polymeric scaffolds with stem cells derived from fetal and adult tissues significantly enhanced healing of large segmental bone defects; however, QD labeling of stem cells eliminated the observed therapeutic effect and failed to conclusively track stem cell location long-term in vivo.

bone tissue engineering | cell tracking | in vivo | quantum dots | stem cells

Delivery of stem cells to treat degenerative conditions or tissue injuries is an attractive care modality because these cells can expand to large population sizes and, given the proper stimuli, differentiate into a variety of tissue types that can enhance the healing process. Although a variety of systemic and local site specific stem cell delivery methods have been investigated, the optimal delivery strategy is unclear, and much about the relationship between delivery method and the stem cell enhanced healing process remains unknown (1). Delivery of stem cells after bone injury—especially challenging injuries such as fracture nonunions or massive long bone defects—is a potential alternative to the large number of bone grafting operations performed annually (2–4). Stem cell delivery may be a particularly effective treatment choice for patients with a compromised supply of endogenous osteogenic or osteoprogenitor cells (5). Although various stem cell sources have been investigated for bone regeneration, few comparative studies have been performed within the same model, and cell distribution and survival after implantation have not been determined (6).

Adult stem cells, and in particular bone marrow derived mesenchymal stem cells (MSCs), have been used to treat long bone segmental defects in rats (7) and dogs (8, 9), and also in human clinical trials (10). However, MSCs have drawbacks including reduced availability with age (11) and cell senescence with loss of multilineage differentiation capability after 34–50 population doublings due to telomere shortening (12).

Fetal stem cells, and in particular amniotic fluid stem (AFS) cells, present an attractive alternative cell source to MSCs for use in tissue engineering therapies. Amniotic fluid, which can be obtained through routine amniocentesis, contains subpopulations of multipotent progenitor cells (13, 14). These cells express many but not all of the markers of embryonic stem cells (ESCs), require no feeder layers for culture, have not been observed to form teratomas in vivo, are capable of >300 population doublings in culture due to preservation of telomere length, and can differentiate into cell types from all three germ layers in vitro, including osteogenic, adipogenic, myogenic, neurogenic, endothelial, and hepatic phenotypes (14). Use of AFS cells also circumvents the controversy associated with the use of ESCs. hAFS cells have been shown to readily produce robust mineralized matrix within 3D porous polymer scaffolds both in vitro and ectopically in vivo (15, 16). Finally, in direct comparisons to hMSCs, hAFS cells have shown superior hepatic differentiation potential (17).

A thorough evaluation of cell-mediated bone segmental defect repair should not only assess restoration of bone form and function but also ascertain whether delivered cells remain at the defect site and contribute to bone healing (18). Culturing cells with quantum dots (QDs) is a facile method commonly used for cell labeling and in vivo tracking. These fluorescent semiconductor nanocrystals have wide excitation spectrums, narrow emission spectra, and long fluorescence decay lifetimes (19). QDs are photostable so they maintain a high level of brightness (10–20 times higher than fluorescent proteins) with limited photobleaching (20). Several in vitro studies using hMSCs have demonstrated highly efficient cell internalization of QDs with no measurable effects on cell viability or function when used at low concentrations (18, 21, 22). However, at least one in vitro study reported that QD internalization into hMSCs impaired their osteogenic differentiation capacity (22). In vivo, fluorescence from QD-loaded cells has been observed for at least 2 months after delivery (23, 24) with no apparent deleterious effects on the health of host animals. Toxic side effects remain a concern, however, because commonly used QDs are composed of a CdSe core surrounded by a biologically inert ZnS shell, and degradation of the shell could expose cells to the core's toxic Cd.

Author contributions: K.M.D., A.J.G., and R.E.G. designed research; K.M.D., K.S., H.Y.S., J.D.B., and R.E.G. performed research; A.J.G. contributed new reagents/analytic tools; K.M.D. analyzed data; and K.M.D. wrote the paper.

The authors declare no conflict of interest.

This article is a PNAS Direct Submission. S.F.B. is a guest editor invited by the Editorial Board.

[1]To whom correspondence should be addressed. E-mail: robert.guldberg@me.gatech.edu.

This article contains supporting information online at www.pnas.org/cgi/content/full/0905444107/DCSupplemental.

Additionally, the fidelity of QD cell tracking in vivo is unclear. Although QDs reportedly do not transfer between live cells (23), they may be released from cells that die after transplantation and produce a false positive signal.

The goals of this study were to (*i*) quantitatively assess the ability of human fetal and adult stem cells to promote segmental bone defect repair, and (*ii*) noninvasively track QD-labeled cells in vivo to determine their biodistribution during the bone healing process. We hypothesized that augmenting the number of viable stem cells at the injury site would significantly enhance functional repair of bone defects in a developmental stage dependent manner and that labeling stem cells with QDs would provide an effective means of tracking their distribution during the bone repair process.

Results

Comparison of Human Stem Cell Sources During Segmental Bone Defect Repair. Femoral segmental defects were treated by implanting acellular scaffolds or scaffolds seeded with hMSCs or hAFS cells. Eight weeks after surgery, bone bridged 0/8 defects treated with scaffolds only, 4/9 defects treated with hMSC-seeded scaffolds, and 1/9 defects treated with hAFS cell-seeded scaffolds, as assessed by double-blind evaluations of 2D x-ray images (Fig. 1*A*). No further bridging occurred by week 12. Micro-CT quantification of bone volume showed no statistically significant differences between cell sources at 8 or 12 weeks, and therefore the hMSC and hAFS cell groups were combined (Fig. 1*B*). Combination of the two cellular groups revealed significantly higher bone volume and maximum torque associated with cell delivery compared to acellular controls (Fig. 1*C*). An in vitro DNA assay showed no significant differences in DNA content per scaffold between the two cell sources, indicating that implanted constructs initially contained similar cell numbers (Fig. 1*D*).

Labeling Stem Cells with Fluorescent QDs. Fluorescence microscopy images revealed a clear fluorescent signal in all wells containing QD-loaded MSCs (Fig. S1*A*). Two different types of QDs were investigated. Although there qualitatively appeared to be minimal differences in fluorescence between QD types and even between different QD concentrations, an 18-hr QD incubation increased QD internalization compared to a 1-hr incubation. QDs were distributed within the cytoplasmic space but not within the nuclei.

When plates were imaged using an IVIS Lumina system, increased fluorescence was confirmed in cells exposed to QDs for 18 h compared with 1 h (Fig. S1*B*). There was also a difference in fluorescence between QD types, with the cells loaded with QTracker QDs emitting a stronger signal than those loaded with QDot ITK QDs. Both fluorescence microscopy and IVIS imaging showed a clear fluorescent signal in QD-loaded rat MSCs, hMSCs, and hAFS cells, indicating QD uptake in multiple stem cell sources and species (Fig. S2).

Live/Dead staining revealed that all QD-loaded stem cells remained viable except for one particular group, the QTracker-loaded rMSCs at the highest QD concentration of 20 nM (Fig. S3*A*). This finding agrees with the literature that QDs can have cytotoxic effects in vitro but generally only at higher concentrations. Based on our in vitro results, we opted for incubating cells in 5 nM QTracker 800 QDs for 18 h for our in vivo stem cell tracking experiments. Finally, QDs did not reduce in vitro hMSC osteogenic differentiation as assessed by qualitatively comparable mineral formation to QD-free hMSCs after Von Kossa assay (Fig. S3*B*).

QD Tracking During Segmental Bone Repair Preliminary Study. Immediately after implantation, IVIS scans revealed a clear fluorescent signal at right hindlimb defect sites that received scaffolds seeded with QD-labeled stem cells (Fig. 2*A*). After 1 week, a signal was detected not only at the right hindlimb sites, but also at the left hindlimb control sites that originally received only acellular scaffolds. Defect-site fluorescent signal intensity decreased rapidly within the first 3 weeks of the study and then decreased slowly during the rest of the study, but remained above background levels (Fig. 2*B*). Significant differences in fluorescent intensity were observed between defects treated with cells and control defects through the first week of the study (Fig. 2*C*). Observed fluorescence patterns and intensities were similar for all animals, regardless of stem cell source. There were no observed signs of negative effects from QDs on animal morbidity or mortality.

The presence of fluorescent QDs was confirmed in histological cryosections, which revealed QDs surrounding DAPI-stained cell nuclei within the PCL scaffold (Fig. S4*A*). QD concentration was qualitatively higher in the right hindlimb defect sites originally implanted with QD-loaded cells, and QDs in the defects originally treated with acellular scaffolds were primarily located near the scaffold interface with the bordering fibrous tissue. QDs were also detected in the kidneys as well as the organs of the reticuloendothelial system (RES) including the liver, spleen, and lymph

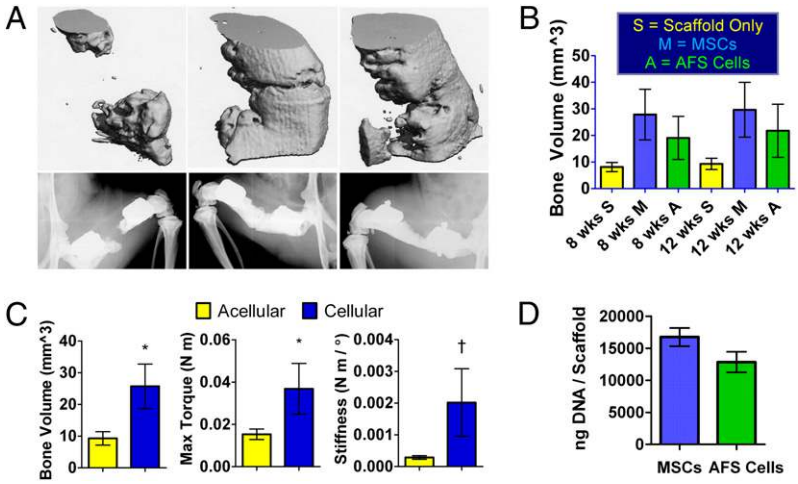

Fig. 1. Structure/function results from in vivo delivery of stem cell-loaded scaffolds. (*A*) Micro-CT (*Upper*) and x-ray (*Lower*) images of the best bone formation per group in defects receiving acellular scaffold (*Left*), hMSC-seeded scaffold (*Center*), or hAFS cell-seeded scaffold (*Right*). (*B*) In vivo bone volume comparison showing no significant differences between groups. (*C*) Pooling of scaffolds loaded with cells revealed significantly higher in vivo bone volume and postmortem torsional strength after 12 weeks compared to acellular scaffolds. (*D*) Similar DNA masses per scaffold indicate initial loading of comparable cell quantities. *, $P < 0.05$; †, $P = 0.06$.

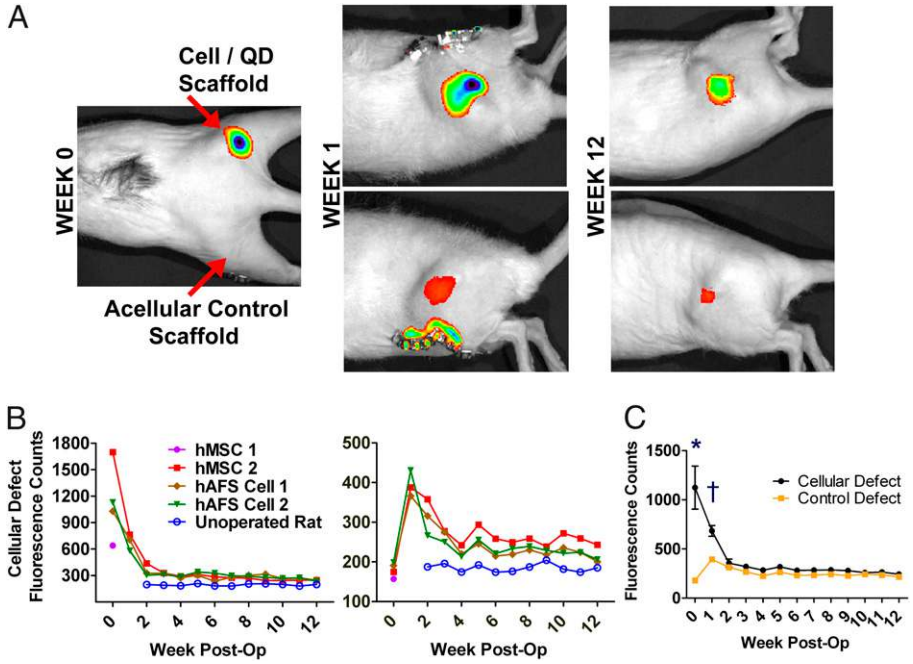

Fig. 2. In vivo QD fluorescence—preliminary study. (*A*) Initial signal observed only at right hindlimb defect site, but after 1 week and for remainder of study the signal was present in both right and left hindlimbs. (*B*) Fluorescence intensity quantification; note the peak in control hindlimb fluorescence after 1 week. Fluorescence count values remained above background levels observed in an unoperated control rat. (*C*) Comparison of fluorescence intensity. $n = 4$ per defect group at week 0 and $n = 3$ at all other times. *, $P < 0.001$; †, $P < 0.05$.

nodes, although at qualitatively lower concentrations than in either defect site (Fig. S4*B*).

QD Tracking During Segmental Bone Repair Live/Devitalized QD-hMSCs Study. Immediately after surgery a fluorescent signal was detected at defect sites treated with either live or devitalized constructs containing QD-labeled cells but not at the contralateral sites treated with acellular scaffolds. After 10 days, all defect sites displayed a clear fluorescent signal, including those treated with acellular scaffolds contralateral to defects treated with QD-containing devitalized hMSCs or human embryonic kidney 293 (HEK) cells (Fig. 3). Immunostaining was performed to identify the cell types that were associated with the QDs. An antibody specific for human nuclei (HuNu) was first shown to effectively label hMSCs in 2D in vitro conditions (Fig. 4*A*). Analysis of histological tissue sections taken from defects treated with live hMSCs, devitalized hMSCs, or HEK cells, as well as their contralateral defects, revealed positive HuNu/QD staining in only the live hMSCs and HEK cells implantation sites (Fig. 4*B*). However, staining with a rat CD68 macrophage antibody revealed extensive positively stained cells in all groups (Fig. 4*C*). At the cell delivery defect site, QDs were found both colocalized with and independent of the stained macrophages in the live hMSC and live HEK constructs but not the devitalized hMSC constructs. Interestingly, the acellular site contralateral to the live hMSC construct also contained QDs colocalized with and independent from the stained macrophages. In contrast, the acellular sites contralateral to dead hMSC or live HEK constructs only contained QDs associated with macrophages.

Unlike the previous QD-free study, no defects were bridged by 12 wks (Fig. 5*A*). There were no differences in average defect bone volume, maximum torque, and torsional stiffness between groups (Fig. 5*B*). The values observed from the QD-free hMSC treated defects used in the first experiment are shown as dashed black lines. There were no observed signs of negative effects from QDs on animal morbidity or mortality.

Discussion

Cellular activity is a vital component of the large bone defect healing process. In this study, delivery of stem cells on a porous polymer scaffold to bone defect sites led to an increase in bone formation and mechanical properties compared to defects receiving scaffold alone. No significant differences in defect bone volume or femoral mechanical properties were observed between adult or fetal stem cell sources. Although stem cell delivery significantly enhanced bone ingrowth and biomechanical properties, consistent bone bridging was not observed. This may be due to the challenging nature of the 8 mm defect model, which is larger than the standard critical size required for nonunion in untreated controls. Other investigators have used rat femoral defects of 5 mm length or less in both immunocompetent (25) and immunocompromised (26) rats. Stem cell-seeded porous polymer scaffold treatment of less challenging 5 mm femoral defects or craniofacial defects, such as in the calvaria, would likely result in a more robust bone repair response (27).

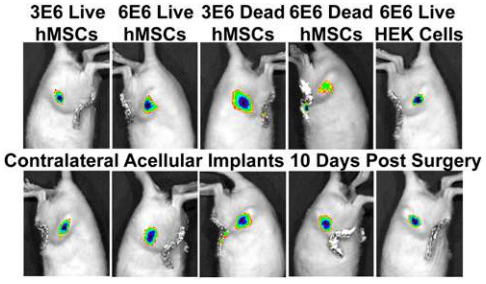

Fig. 3. In vivo QD fluorescence—live versus devitalized hMSCs study. Femoral bone defects were treated by delivery of scaffolds containing either 3E6 or 6E6 QD-loaded live hMSCs, 3E6 or 6E6 QD-loaded devitalized hMSCs, or 6E6 QD-loaded HEK cells, with contralateral defects receiving acellular scaffolds only. Ten days later, all defects displayed a clear fluorescent signal.

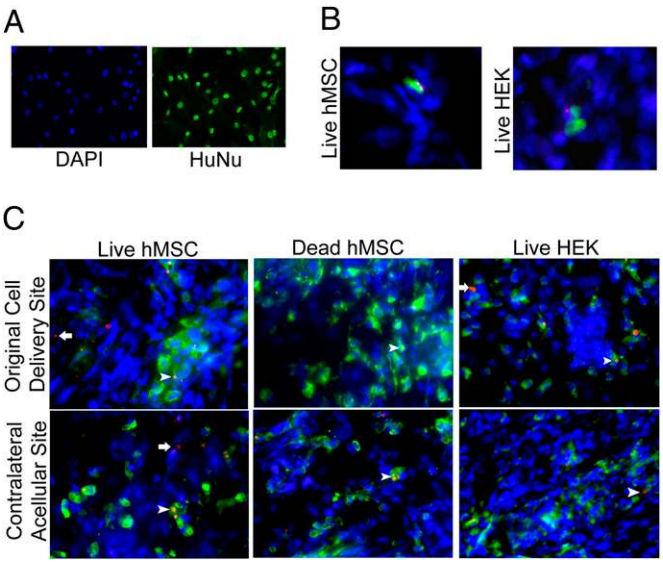

Fig. 4. Immunolabeling to identify cell types associated with QDs. (*A*) Two-dimensional in vitro labeling of hMSCs with DAPI and HuNu human nuclear antibody. (Magnification: 20×.) (*B*) Cells labeled with HuNu from defects treated with 6E6 live hMSCs or 6E6 HEK cells. Green, hMSCs; blue, DAPI; red, QDs. (Magnification: 40×.) (*C*) Cells labeled with CD68 rat macrophage antibody. Green, macrophages; blue, DAPI; red, QDs. Arrowheads point to QDs colocalized with macrophages; arrows point to QDs separate from macrophages. (Magnification: 40×.)

For cell-mediated repair of challenging defects, it may also be necessary to co-deliver programming cues that direct delivered stem cells to osteogenically differentiate. Co-delivered osteogenic signals may be particularly effective for pluripotent fetal AFS cells, which are believed to be more primitive than the more specialized multipotent adult MSCs.

Functional regeneration of the bone defects may also have been limited by short-term cell viability or cell migration from defect sites. This possibility led us to investigate the fate of delivered cells by labeling them with QDs. In a preliminary study, we observed strong QD fluorescence in vivo at the defect site for at least 12 weeks after implantation of scaffolds seeded with QD-loaded stem cells. Interestingly, contralateral defect sites treated with acellular scaffolds began to display clear fluorescent signals 1 week after implantation, suggesting the possibility that delivered QD-containing stem cells may have homed to the area of tissue damage, which has been reported by multiple groups as an ability of hMSCs (1). The presence of QDs at defect sites and in RES organs was confirmed by histology. Observing QDs in RES organs substantiated reports that free QDs would not enter neighboring cells but rather enter the circulation and become sequestered in RES organs (23, 24, 28).

To confirm that QDs were in fact associated with the delivered stem cells in both original delivery and initially acellular contralateral sites, a second study was performed in which scaffolds were implanted that contained either live or devitalized QD-loaded hMSCs or QD-loaded non-stem HEK cells. The observation of contralateral fluorescence in all defect sites after 10 days suggested that, at least in the devitalized group, QDs were no longer associated with hMSCs because dead cells would have no ability to migrate. Immunostaining revealed that although a small population of QDs was still associated with hMSCs in the live cell and HEK cell groups, the majority of QDs in all groups were associated with host macrophage cells. This finding agrees with a previous report that QTracker 565 QDs injected into mice accumulated in murine $CD68^+$ macrophages in atherosclerotic legions (29). The mechanism through which QDs delivered at one local injury became associated with macrophages in a separate local injury site remains unclear. Additionally, although 5 nM QD-labeling caused no observed negative effects on cell viability or osteogenic differentiation capacity in vitro, QD-loaded live hMSCs failed to enhance bone formation or bridge any defects. This is in contrast to the previous study without QDs, in which there was a significant effect of stem cell implantation on bone ingrowth and biomechanical properties and bridging was observed in 4/9 animals receiving hMSCs.

In conclusion, human stem cells seeded on polymer scaffolds and delivered to nude rat critically sized segmental bone defects enhanced bone repair compared to treatment with acellular scaffolds; however, no differences in healing were observed between fetal and adult stem cell sources. Although stem cell delivery improved bone defect repair, consistent bridging was not observed, likely because of a lack of long-term retention of live cells at the defect site. This study further identified limitations associated with using QD labeling for noninvasive tracking of delivered stem cells. Improved methods of noninvasive cell tracking that do not alter cell function in vivo are needed to optimize stem cell delivery strategies and compare the effectiveness of different stem cell sources for tissue regeneration. Future studies will explore alternate in vivo cell tracking modalities, such as genetic modification of stem cells to express green fluorescent protein and/or luciferase, as well as investigate improvements to the stem cell mediated healing response by the addition of co-delivered osteogenic cues to push stem cells to osteogenically differentiate and increase matrix mineralization.

Materials and Methods

Scaffold Preparation. Sterile Poly(ε-caprolactone) (PCL) (Osteopore International) cylindrical scaffolds, 9 mm in height, 5 mm in Ø, and of 85% porosity were soaked in a solution of the collagen-mimetic peptide GFOGER and then coated with lyophilized type I collagen (Vitrogen 100; Cohesion Technologies) to increase cell adhesion and help mediate the osteogenic response of MSCs (30) and AFS cells. More detailed descriptions for all sections are available in *SI Materials and Methods*.

Cell Culture. For segmental defect studies, hMSCs and hAFS cells were seeded on tissue culture plates and grown to near-confluence. For QD segmental defect studies, hMSCs, hAFS cells, or HEK cells were incubated in a 5 nM solution of QTracker 800 QDs (Invitrogen) for 18 h. Either 3E6 (hMSCs/hAFS cells) or 6E6 (hMSCs/HEK) QD-labeled cells were seeded onto PCL scaffolds described above

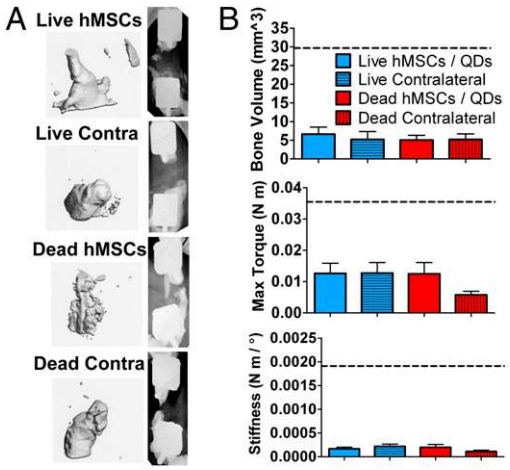

Fig. 5. Structure/function results from in vivo delivery of live or devitalized QD-loaded hMSCs. (*A*) Micro-CT (*Left*) and x-ray (*Right*) images of the best bone formation per group in defects receiving live hMSCs, acellular scaffold contralateral to live hMSCs, devitalized hMSCs, or acellular scaffold contralateral to devitalized hMSCs. (*B*) Twelve-week in vivo bone volume and postmortem defect maximum torque and torsional stiffness. Black dashed lines indicate values for the QD-free hMSC treated defects from the segmental defect study without QDs.

and cultured until implantation. Some QD-labeled hMSC scaffolds were exposed to devitalizing freeze–thaw cycles. For the defect study without QDs, 3E6 cells were seeded on scaffolds and cultured until implantation.

For 2D in vitro QD studies, 20,000 rat MSCs were seeded in wells of eight-well Lab-Tek plates and loaded with 5, 10, or 20 nM solutions of QTracker 800 QDs or QDot ITK 800 QDs (Invitrogen) for either 1 or 18 h. The QTracker QDs feature amino-PEGylation surface coatings giving them a positive charge, whereas the QDot ITK QDs are coated with carboxyl surface groups giving them a negative charge. Additionally, some wells were stained with DAPI nuclear stain. Next rMSCs, hMSCs, and hAFS cells were loaded with QDs at concentrations of 0, 10, 15, and 20 nM for 18 h and then stained with DAPI or with Live/Dead stain (consisting of calcein/ethidium; Invitrogen) to assess cell viability. To assess QD effects on osteogenic differentiation, 1,000 hMSCs were seeded on six-well culture plates and grown to confluence. 0.5 mL of 5 nM QTracker QDs was then added to half of the wells for 18 h. Plates were cultured for 3 weeks in culture media supplemented with osteogenic factors (1 nM dexamethasone, 6 mM β-glycerol phosphate, 50 μg/mL ascorbic acid 2-phosphate, 50 ng/mL L-thyroxine), and then a Von Kossa assay was performed to assess mineral formation.

For 2D in vitro human cell nuclear labeling, 100,000 hMSCs were seeded on single-well Lab-Tek plates and then immunostained with mouse anti-human nuclear antigen monoclonal antibody (HuNu) (Millipore, MAB1281). Next, a fluorescent Alexa Fluor 488 donkey anti-mouse (Invitrogen) secondary antibody was applied, followed by DAPI counterstaining.

DNA Analysis. Three days after seeding cells for the segmental defect studies as mentioned above, extra scaffolds with QD-free cells were used to quantify DNA. Scaffolds were dried and digested with Proteinase K, followed by DNA quantification using a PicoGreen assay (Quant-iT PicoGreen dsDNA Kit; Invitrogen).

Surgical Technique. All surgical techniques were approved by the Georgia Institute of Technology Institutional Animal Care and Use Committee (Protocol A08032). Female 13-week-old athymic rats (RNU Nude; Charles River Laboratories) were anesthetized by using isoflurane. Bilateral 8-mm critically sized femoral defects were then created and stabilized by novel custom modular fixation plates described previously (31, 32). In the QD-free study, PCL scaffolds, with or without cells, were press fitted into the defects before closing the wound site. Rats received bilateral combinations of either acellular scaffold (n = 8), hMSC-seeded scaffold (n = 9), or hAFS cell-seeded scaffold (n = 9). In both in vivo QD studies, rats were implanted with scaffolds containing QD-labeled cells in one hindlimb defect and acellular scaffolds in the contralateral defect. In the preliminary QD study, two rats were treated with hMSCs and two rats with hAFS cells. In the QD study comparing live and devitalized cells, 10 rats were treated with scaffolds containing live hMSCs (n = 5 3E6 cells/n = 5 6E6 cells), 10 rats were treated with scaffolds containing devitalized hMSCs (n = 5 3E6 cells/n = 5 6E6 cells), and 2 rats were treated with 6E6 HEK cells. Rats were given injections of buprenorphine through 72 h postsurgery for pain relief. Animals resumed normal ambulation and behavior within 3 days, except for one rat in the preliminary QD study that failed to recover because of misplacement of the internal fixator plate, leading to its euthanization after 4 days.

X-Ray and Microcomputed Tomography (Micro-CT) Imaging. Qualitative bone growth into defect sites was assessed by 2D in vivo digital x-rays (Faxitron MX-20 Digital; Faxitron X-Ray) taken 4, 8, and 12 weeks after surgery. For the QD-free study and the QD study comparing live and devitalized cells, quantitative bone formation was assessed by 3D micro-CT scans (Viva-CT 40; Scanco Medical) of femurs both in vivo at 8 and 12 weeks after surgery and by postmortem ex vivo scans. After scanning, a constant volume of interest (VOI) was centered over the defect site for quantitative analysis of samples.

Torsional Mechanical Testing. For both the QD-free study (n = 8 acellular scaffold group, n = 9 per stem cell group) and the QD live versus devitalized cells study (n = 9 each for the live, live contralateral, devitalized, and devitalized contralateral groups), after postmortem micro-CT imaging, femur ends were potted in custom mounting blocks and loaded onto an ELF 3200 ElectroForce torsion testing system (Bose Corporation). Next, the polysulfone bridging plate that had shielded defects from loads and damage was removed. Finally, a torsional load was applied to the femur and maximum torque and torsional stiffness were recorded through 90° rotation.

Preparation of Histological Cryosections. All rats from the preliminary QD study were killed 12 weeks after surgery and had their femurs, kidneys, and organs of the reticuloendothelial system (spleen, liver, lymph nodes) harvested. Tissues were frozen, and 50-μm tissue sections were taken by using a Microm Cryo-Star HM 560MV cryostat (Thermo Fisher) and attached to Superfrost Plus slides. Glass coverslips were mounted by using ProLong Gold antifade mounting medium with DAPI (Invitrogen) to visualize cell nuclei. In the live versus devitalized cell QD study, one rat each from the live hMSC group, devitalized hMSC group, and HEK group was killed 4 weeks after surgery. Femurs were frozen and sectioned in 20-μm slices. Sections prepared for human nuclei staining were stained with HuNu primary antibody (Millipore, MAB1281). Sections prepared for rat macrophage staining were stained with a mouse anti-rat CD68 primary antibody (AbD Serotec, MCA341R). Next, a fluorescent Alexa Fluor 488 donkey anti-mouse (Invitrogen) secondary antibody was applied to all sections followed by DAPI counter staining. Control sections for each immunolabel excluded primary antibody staining.

Fluorescence Microscopy. Fluorescent images of cells in Lab-Tek plates and of tissue cryosections were obtained by using a Zeiss Axio Observer inverted microscope equipped with a specialized Qdot 800 filter set (Chroma 32021; Chroma Technology).

IVIS Fluorescent Imaging. Fluorescent images of eight-well plates were obtained by using an IVIS Lumina imaging system (Caliper Life Sciences). For the preliminary in vivo QD study, fluorescent scans were performed immediately after surgery and then weekly for 12 weeks. For the live versus devitalized cell study, scans were performed immediately after surgery and then after 10, 20, 40, 60, and 80 days. Fluorescent count values were measured by using a uniform circular region of interest applied at hindlimb defect sites.

Statistical Analysis. For the comparison of defect bone volume and mechanical properties, one-way analysis of variance was performed in Minitab (Minitab Inc.) using a general linear model with Tukey pairwise post hoc tests. For the comparison of defect site QD fluorescence, repeated-measures two-way analysis of variance was performed with Bonferroni post tests in Prism 5 (GraphPad Software).

ACKNOWLEDGMENTS. We thank Darwin Prockop (Texas A&M University) for the supply of hMSCs, Anthony Atala (Wake Forest University) for the supply of hAFS cells, and W. Robert Taylor (Emory University/Georgia Institute of Technology) for guidance on the quantum dot studies. This work was supported by National Institutes of Health Grants R01 AR051336 and R01 AR056694, National Science Foundation Grant EEC-9731643, and K.M.D. received support from a National Science Foundation Graduate Research Fellowship.

1. Chamberlain G, Fox J, Ashton B, Middleton J (2007) Concise review: mesenchymal stem cells: their phenotype, differentiation capacity, immunological features, and potential for homing. *Stem Cells* 25:2739–2749.
2. Song L, Tuan RS (2004) Transdifferentiation potential of human mesenchymal stem cells derived from bone marrow. *FASEB J* 18:980–982.
3. Jaiswal N, Haynesworth SE, Caplan AI, Bruder SP (1997) Osteogenic differentiation of purified, culture-expanded human mesenchymal stem cells in vitro. *J Cell Biochem* 64:295–312.
4. Bucholz RW (2002) Nonallograft osteoconductive bone graft substitutes. *Clin Orthop Relat Res* (395):44–52.
5. Bruder SP (1999) Tissue engineering of bone. Cell based strategies. *Clin Orthop Relat Res* 367S:S68–S83.
6. Waese EY, Kandel RA, Kandel RR, Stanford WL (2008) Application of stem cells in bone repair. *Skeletal Radiol* 37:601–608.
7. Bruder SP, et al. (1998) Bone regeneration by implantation of purified, culture-expanded human mesenchymal stem cells. *J Orthop Res* 16:155–162.
8. Bruder SP, Kraus KH, Goldberg VM, Kadiyala S (1998) The effect of implants loaded with autologous mesenchymal stem cells on the healing of canine segmental bone defects. *J Bone Joint Surg Am* 80:985–996.
9. Arinzeh TL, et al. (2003) Allogeneic mesenchymal stem cells regenerate bone in a critical-sized canine segmental defect. *J Bone Joint Surg Am* 85-A:1927–1935.
10. Quarto R, et al. (2001) Repair of large bone defects with the use of autologous bone marrow stromal cells. *N Engl J Med* 344:385–386.
11. Caplan AI (2004) Mesenchymal stem cells. *Handbook of Stem Cells.* (Elsevier Academic, New York), Vol 2, pp 299–308.
12. Derubeis AR, Cancedda R (2004) Bone marrow stromal cells (BMSCs) in bone engineering: limitations and recent advances. *Ann Biomed Eng* 32:160–165.
13. Tsai MS, Lee JL, Chang YJ, Hwang SM (2004) Isolation of human multipotent mesenchymal stem cells from second-trimester amniotic fluid using a novel two-stage culture protocol. *Hum Reprod* 19:1450–1456.
14. De Coppi P, et al. (2007) Isolation of amniotic stem cell lines with potential for therapy. *Nat Biotechnol* 25:100–106.
15. Peister A, Deutsch ER, Kolambkar Y, Hutmacher DW, Guldberg R (2009) Amniotic fluid stem cells produce robust mineral deposits on biodegradable scaffolds. *Tissue Eng Part A* 15: 3129–3138.
16. Guldberg RE, et al. (2007) Biologic augmentation of polymer scaffolds for bone repair. *J Musculoskelet Neuronal Interact* 7:333–334.

17. Zheng YB, et al. (2008) Characterization and hepatogenic differentiation of mesenchymal stem cells from human amniotic fluid and human bone marrow: a comparative study. *Cell Biol Int* 32:1439–1448.
18. Shah BS, Clark PA, Moioli EK, Stroscio MA, Mao JJ (2007) Labeling of mesenchymal stem cells by bioconjugated quantum dots. *Nano Lett* 7:3071–3079.
19. Jamieson T, et al. (2007) Biological applications of quantum dots. *Biomaterials* 28: 4717–4732.
20. Alivisatos AP (1996) Semiconductor clusters, nanocrystals, and quantum dots. *Science* 271:933–937.
21. Seleverstov O, et al. (2006) Quantum dots for human mesenchymal stem cells labeling. A size-dependent autophagy activation. *Nano Lett* 6:2826–2832.
22. Hsieh SC, et al. (2006) The inhibition of osteogenesis with human bone marrow mesenchymal stem cells by CdSe/ZnS quantum dot labels. *Biomaterials* 27:1656–1664.
23. Rosen AB, et al. (2007) Finding fluorescent needles in the cardiac haystack: tracking human mesenchymal stem cells labeled with quantum dots for quantitative in vivo three-dimensional fluorescence analysis. *Stem Cells* 25:2128–2138.
24. Voura EB, Jaiswal JK, Mattoussi H, Simon SM (2004) Tracking metastatic tumor cell extravasation with quantum dot nanocrystals and fluorescence emission-scanning microscopy. *Nat Med* 10:993–998.
25. Yasko AW, et al. (1992) The healing of segmental bone defects, induced by recombinant human bone morphogenetic protein (rhBMP-2). A radiographic, histological, and biomechanical study in rats. *J Bone Joint Surg Am* 74:659–670.
26. Jäger M, et al. (2007) Bone healing and migration of cord blood-derived stem cells into a critical size femoral defect after xenotransplantation. *J Bone Miner Res* 22: 1224–1233.
27. Guldberg RE, et al. (2004) Functional integration of tissue-engineered bone constructs. *J Musculoskelet Neuronal Interact* 4:399–400.
28. Ballou B, Lagerholm BC, Ernst LA, Bruchez MP, Waggoner AS (2004) Noninvasive imaging of quantum dots in mice. *Bioconjug Chem* 15:79–86.
29. Buono C, Anzinger JJ, Amar M, Kruth HS (2009) Fluorescent pegylated nanoparticles demonstrate fluid-phase pinocytosis by macrophages in mouse atherosclerotic lesions. *J Clin Invest* 119:1373–1381.
30. Reyes CD, Petrie TA, Burns KL, Schwartz Z, García AJ (2007) Biomolecular surface coating to enhance orthopaedic tissue healing and integration. *Biomaterials* 28:3228–3235.
31. Oest ME, Dupont KM, Kong HJ, Mooney DJ, Guldberg RE (2007) Quantitative assessment of scaffold and growth factor-mediated repair of critically sized bone defects. *J Orthop Res* 25:941–950.
32. Rai B, et al. (2007) Combination of platelet-rich plasma with polycaprolactone-tricalcium phosphate scaffolds for segmental bone defect repair. *J Biomed Mater Res A* 81:888–899.